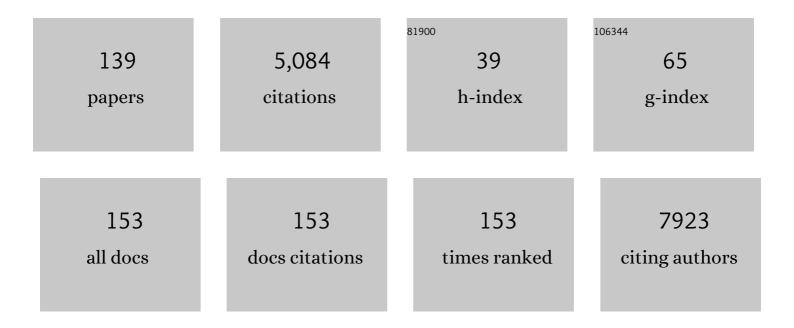
List of Publications by Year in descending order

Source: https://exaly.com/author-pdf/5155260/publications.pdf Version: 2024-02-01



#	Article	IF	CITATIONS
1	Correlating the electronic structure of perovskite La1â^'Sr CoO3 with activity for the oxygen evolution reaction: The critical role of Co 3d hole state. Journal of Energy Chemistry, 2022, 65, 637-645.	12.9	39
2	Optimization of SnO <sub>2</sub> electron transport layer for efficient planar perovskite solar cells with very low hysteresis. Materials Advances, 2022, 3, 456-466.	5.4	20
3	A Heterogenized Copper Phenanthroline System to Catalyze the Oxygen Reduction Reaction. ChemElectroChem, 2022, 9, .	3.4	3
4	Mesoporous High-Entropy Oxide Thin Films: Electrocatalytic Water Oxidation on High-Surface-Area Spinel (Cr <sub>0.2</sub> Mn <sub>0.2</sub> Fe <sub>0.2</sub> Co <sub>0.2</sub> Ni <sub>0.2</sub> ) <sub>3</sub> C Electrodes. ACS Applied Energy Materials, 2022, 5, 717-730.	<\$11 \$11 \$4 </td <td>sub&gt;</td>	sub>
5	A Selective Copper Based Oxygen Reduction Catalyst for the Electrochemical Synthesis of H 2 O 2 at Neutral pH. ChemElectroChem, 2022, 9, .	3.4	7
6	Toward Understanding the Short ircuit Current Loss in Perovskite Solar Cells with 2D Passivation Layers. Solar Rrl, 2022, 6, .	5.8	8
7	Potassium hydride-intercalated graphite as an efficient heterogeneous catalyst for ammonia synthesis. Nature Catalysis, 2022, 5, 222-230.	34.4	37
8	On the Homogeneity of a Cobalt-Based Water Oxidation Catalyst. ACS Catalysis, 2022, 12, 4597-4607.	11.2	14
9	Predoped Oxygenated Defects Activate Nitrogen-Doped Graphene for the Oxygen Reduction Reaction. ACS Catalysis, 2022, 12, 173-182.	11.2	17
10	Thickness and Morphology Dependent Electrical Properties of ALD‣ynthesized MoS <sub>2</sub> FETs. Advanced Electronic Materials, 2022, 8, .	5.1	9
11	High-entropy transition metal chalcogenides as electrocatalysts for renewable energy conversion. Current Opinion in Electrochemistry, 2022, 34, 101010.	4.8	22
12	A Multiâ€Functional Separator for Liâ€S Batteries: WS <sub>2</sub> @C Nanoflowers Catalyze the Rapid Recycling of Lithium Polysulfides by Polar Attraction. ChemElectroChem, 2022, 9, .	3.4	2
13	Imaging the facet surface strain state of supported multi-faceted Pt nanoparticles during reaction. Nature Communications, 2022, 13, .	12.8	11
14	(Digital Presentation) Investigation of Reversal Tolerant Anode Catalysts Ageing during Start-up/Shut-Down Events on a PEM Fuel Cell. ECS Meeting Abstracts, 2022, MA2022-01, 1467-1467.	0.0	0
15	Hydrogen-efficient non-oxidative transformation of methanol into dimethoxymethane over a tailored bifunctional Cu catalyst. Sustainable Energy and Fuels, 2021, 5, 117-126.	4.9	11
16	Phosphate-assisted efficient oxygen evolution over finely dispersed cobalt particles supported on graphene. Catalysis Science and Technology, 2021, 11, 1039-1048.	4.1	2
17	Promoting oxygen evolution of IrO2 in acid electrolyte by Mn. Electrochimica Acta, 2021, 366, 137448.	5.2	21
18	On the Stability of Co <sub>3</sub> O <sub>4</sub> Oxygen Evolution Electrocatalysts in Acid. ChemCatChem. 2021, 13, 459-467.	3.7	32

#	Article	IF	CITATIONS
19	Two birds with one stone: dual grain-boundary and interface passivation enables >22% efficient inverted methylammonium-free perovskite solar cells. Energy and Environmental Science, 2021, 14, 5875-5893.	30.8	180
20	Nanoscale Hybrid Amorphous/Graphitic Carbon as Key Towards Nextâ€Generation Carbonâ€Based Oxidative Dehydrogenation Catalysts. Angewandte Chemie - International Edition, 2021, 60, 5898-5906.	13.8	37
21	The electronic structure of transition metal oxides for oxygen evolution reaction. Journal of Materials Chemistry A, 2021, 9, 19465-19488.	10.3	90
22	ldentification of Photoexcited Electron Relaxation in a Cobalt Phosphide Modified Carbon Nitride Photocatalyst. ChemPhotoChem, 2021, 5, 330-334.	3.0	8
23	Innentitelbild: Nanoskaliger hybrider amorph/graphitischer Kohlenstoff als Schlüssel zur nähsten Generation von kohlenstoffbasierten Katalysatoren für oxidative Dehydrierungen (Angew. Chem.) Tj ETQq1 1 0.	.7 <b>&amp;⊕</b> 314 (	rg <b>B</b> T /Overlo
24	Facetâ€Dependent Strain Determination in Electrochemically Synthetized Platinum Model Catalytic Nanoparticles. Small, 2021, 17, e2007702.	10.0	4
25	CO <sub>2</sub> Hydrogenation to Higher Alcohols over K-Promoted Bimetallic Fe–In Catalysts on a Ce–ZrO <sub>2</sub> Support. ACS Sustainable Chemistry and Engineering, 2021, 9, 6235-6249.	6.7	32
26	Reversible hydrogenation restores defected graphene to graphene. Science China Chemistry, 2021, 64, 1047-1056.	8.2	6
27	Reactive Dual Magnetron Sputtering: A Fast Method for Preparing Stoichiometric Microcrystalline ZnWO4 Thin Films. Surfaces, 2021, 4, 106-114.	2.3	1
28	On the Contact Optimization of ALD-Based MoS <sub>2</sub> FETs: Correlation of Processing Conditions and Interface Chemistry with Device Electrical Performance. ACS Applied Electronic Materials, 2021, 3, 3185-3199.	4.3	8
29	Comparing the Intrinsic HER Activity of Transition Metal Dichalcogenides: Pitfalls and Suggestions. ACS Energy Letters, 2021, 6, 2619-2625.	17.4	47
30	Twin boundary migration in an individual platinum nanocrystal during catalytic CO oxidation. Nature Communications, 2021, 12, 5385.	12.8	14
31	A comprehensive comparative study of CO2-resistance and oxygen permeability of 60Âwt % Ce0.8M0.2O2– (M = La, Pr, Nd, Sm, Gd) - 40Âwt % La0.5Sr0.5Fe0.8Cu0.2O3– dual-phase membranes. Journa of Membrane Science, 2021, 639, 119783.	l 8.2	9
32	Enhanced CO2 methanation activity over La2-xCexNiO4 perovskite-derived catalysts: Understanding the structure-performance relationships. Chemical Engineering Journal, 2021, 426, 131760.	12.7	18
33	Stabilization effects in binary colloidal Cu and Ag nanoparticle electrodes under electrochemical CO <sub>2</sub> reduction conditions. Nanoscale, 2021, 13, 4835-4844.	5.6	29
34	Nanoskaliger hybrider amorph/graphitischer Kohlenstoff als Schlüssel zur nÃ <b>e</b> hsten Generation von kohlenstoffbasierten Katalysatoren für oxidative Dehydrierungen. Angewandte Chemie, 2021, 133, 5962-5971.	2.0	3
35	Effect of proximity and support material on deactivation of bifunctional catalysts for the conversion of synthesis gas to olefins and aromatics. Catalysis Today, 2020, 342, 161-166.	4.4	46
36	Mn promotion of rutile TiO2-RuO2 anodes for water oxidation in acidic media. Applied Catalysis B: Environmental, 2020, 261, 118225.	20.2	53

#	Article	IF	CITATIONS
37	Facile Synthesis of Sulfur ontaining Transition Metal (Mn, Fe, Co, and Ni) (Hydr)oxides for Efficient Oxygen Evolution Reaction. ChemCatChem, 2020, 12, 710-716.	3.7	17
38	Nanoweb Surfaceâ€Mounted Metal–Organic Framework Films with Tunable Amounts of Acid Sites as Tailored Catalysts. Chemistry - A European Journal, 2020, 26, 691-698.	3.3	11
39	Porous nitrogen-doped carbon/carbon nanocomposite electrodes enable sodium ion capacitors with high capacity and rate capability. Nano Energy, 2020, 67, 104240.	16.0	56
40	Assessment of the Location of Pt Nanoparticles in Pt/zeolite Y/γâ€Al <sub>2</sub> O <sub>3</sub> Composite Catalysts. ChemCatChem, 2020, 12, 615-622.	3.7	13
41	Electronic Structure and Interface Energetics of CuBi <sub>2</sub> O <sub>4</sub> Photoelectrodes. Journal of Physical Chemistry C, 2020, 124, 22416-22425.	3.1	39
42	Probing CO <sub>2</sub> Reduction Pathways for Copper Catalysis Using an Ionic Liquid as a Chemical Trapping Agent. Angewandte Chemie - International Edition, 2020, 59, 18095-18102.	13.8	56
43	Probing CO 2 Reduction Pathways for Copper Catalysis Using an Ionic Liquid as a Chemical Trapping Agent. Angewandte Chemie, 2020, 132, 18251-18258.	2.0	6
44	Investigation of the stability of NiFe-(oxy)hydroxide anodes in alkaline water electrolysis under industrially relevant conditions. Catalysis Science and Technology, 2020, 10, 5593-5601.	4.1	35
45	Synthesis of edge-enriched WS2 on high surface area WS2 framework by atomic layer deposition for electrocatalytic hydrogen evolution reaction. Journal of Vacuum Science and Technology A: Vacuum, Surfaces and Films, 2020, 38, .	2.1	4
46	Controlling pore size and pore functionality in sp <sup>2</sup> -conjugated microporous materials by precursor chemistry and salt templating. Journal of Materials Chemistry A, 2020, 8, 21680-21689.	10.3	13
47	Innenrücktitelbild: Probing CO <sub>2</sub> Reduction Pathways for Copper Catalysis Using an Ionic Liquid as a Chemical Trapping Agent (Angew. Chem. 41/2020). Angewandte Chemie, 2020, 132, 18431-18431.	2.0	0
48	Continuous scanning for Bragg coherent X-ray imaging. Scientific Reports, 2020, 10, 12760.	3.3	6
49	Electroless Nanoplating of Iridium: Templateâ€Assisted Nanotube Deposition for the Continuous Flow Reduction of 4â€Nitrophenol. ChemElectroChem, 2020, 7, 3496-3507.	3.4	5
50	Stability of Colloidal Iron Oxide Nanoparticles on Titania and Silica Support. Chemistry of Materials, 2020, 32, 5226-5235.	6.7	6
51	Efficient palladium catalysis for the upgrading of itaconic and levulinic acid to 2-pyrrolidones followed by their vinylation into value-added monomers. Green Chemistry, 2020, 22, 4532-4540.	9.0	13
52	Ligand-free ZnS nanoparticles: as easy and green as it gets. Chemical Communications, 2020, 56, 8707-8710.	4.1	7
53	The Influence of the Ligand in the Iridium Mediated Electrocatalyic Water Oxidation. ACS Catalysis, 2020, 10, 4398-4410.	11.2	32
54	Catalytic Hydrogenation of Renewable Levulinic Acid to Î <sup>3</sup> -Valerolactone: Insights into the Influence of Feed Impurities on Catalyst Performance in Batch and Flow Reactors. ACS Sustainable Chemistry and Engineering, 2020, 8, 5903-5919.	6.7	35

#	Article	IF	CITATIONS
55	Influence of Local Environments in Pores of Different Size on the Catalytic Liquid-Phase Oxidation of <scp>d</scp> -Glucose by Au Nanoparticles Supported on Nanoporous Carbon. ACS Applied Nano Materials, 2020, 3, 7695-7703.	5.0	8
56	Large area, patterned growth of 2D MoS <sub>2</sub> and lateral MoS <sub>2</sub> –WS <sub>2</sub> heterostructures for nano- and opto-electronic applications. Nanotechnology, 2020, 31, 255603.	2.6	46
57	Electrochemical stability of RuO2(110)/Ru(0001) model electrodes in the oxygen and chlorine evolution reactions. Electrochimica Acta, 2020, 336, 135713.	5.2	30
58	Increased activity in the oxygen evolution reaction by Fe <sup>4+</sup> -induced hole states in perovskite La <sub>1â^'x</sub> Sr <sub>x</sub> FeO <sub>3</sub> . Journal of Materials Chemistry A, 2020, 8, 4407-4415.	10.3	78
59	Cu Electrodeposition on Nanostructured MoS <sub>2</sub> and WS <sub>2</sub> and Implications for HER Active Site Determination. Journal of the Electrochemical Society, 2020, 167, 116517.	2.9	5
60	Ni <sup>3+</sup> -Induced Hole States Enhance the Oxygen Evolution Reaction Activity of Ni <sub><i>x</i></sub> Co <sub>3–<i>x</i></sub> O <sub>4</sub> Electrocatalysts. Chemistry of Materials, 2019, 31, 7618-7625.	6.7	76
61	Efficient and Highly Transparent Ultraâ€Thin Nickelâ€Iron Oxyâ€hydroxide Catalyst for Oxygen Evolution Prepared by Successive Ionic Layer Adsorption and Reaction. ChemPhotoChem, 2019, 3, 1050-1054.	3.0	6
62	The Origin of High Activity of Amorphous MoS <sub>2</sub> in the Hydrogen Evolution Reaction. ChemSusChem, 2019, 12, 4383-4389.	6.8	90
63	Hybrid Oleate–Iodide Ligand Shell for Air-Stable PbSe Nanocrystals and Superstructures. Chemistry of Materials, 2019, 31, 5808-5815.	6.7	12
64	Low-Temperature Phase-Controlled Synthesis of Titanium Di- and Tri-sulfide by Atomic Layer Deposition. Chemistry of Materials, 2019, 31, 9354-9362.	6.7	35
65	The Origin of High Activity of Amorphous MoS 2 in the Hydrogen Evolution Reaction. ChemSusChem, 2019, 12, 4336-4336.	6.8	2
66	Influence of Reduced Cu Surface States on the Photoelectrochemical Properties of CuBi <sub>2</sub> O <sub>4</sub> . ACS Applied Energy Materials, 2019, 2, 6866-6874.	5.1	23
67	Template-Free Nanostructured Fluorine-Doped Tin Oxide Scaffolds for Photoelectrochemical Water Splitting. ACS Applied Materials & amp; Interfaces, 2019, 11, 36485-36496.	8.0	17
68	Elucidation of the Structure of a Thiol Functionalized Cu-tmpa Complex Anchored to Gold via a Self-Assembled Monolayer. Inorganic Chemistry, 2019, 58, 13007-13019.	4.0	5
69	<i>In situ</i> structural evolution of single particle model catalysts under ambient pressure reaction conditions. Nanoscale, 2019, 11, 331-338.	5.6	10
70	Edge-Site Nanoengineering of WS <sub>2</sub> by Low-Temperature Plasma-Enhanced Atomic Layer Deposition for Electrocatalytic Hydrogen Evolution. Chemistry of Materials, 2019, 31, 5104-5115.	6.7	57
71	Unraveling the Role of Lithium in Enhancing the Hydrogen Evolution Activity of MoS <sub>2</sub> : Intercalation versus Adsorption. ACS Energy Letters, 2019, 4, 1733-1740.	17.4	45
72	Electrolyte Effects on the Stability of Niâ^'Mo Cathodes for the Hydrogen Evolution Reaction. ChemSusChem, 2019, 12, 3491-3500.	6.8	37

#	Article	IF	CITATIONS
73	Understanding the Charge Storage Mechanism to Achieve High Capacity and Fast Ion Storage in Sodiumâ€Ion Capacitor Anodes by Using Electrospun Nitrogenâ€Doped Carbon Fibers. Advanced Functional Materials, 2019, 29, 1902858.	14.9	79
74	Elucidating the electronic structure of CuWO <sub>4</sub> thin films for enhanced photoelectrochemical water splitting. Journal of Materials Chemistry A, 2019, 7, 11895-11907.	10.3	67
75	Electronic Effects Determine the Selectivity of Planar Au–Cu Bimetallic Thin Films for Electrochemical CO <sub>2</sub> Reduction. ACS Applied Materials & Interfaces, 2019, 11, 16546-16555.	8.0	71
76	Enhancing the electrocatalytic activity of 2H-WS <sub>2</sub> for hydrogen evolution <i>via</i> defect engineering. Physical Chemistry Chemical Physics, 2019, 21, 6071-6079.	2.8	60
77	Towards a quantitative determination of strain in Bragg Coherent X-ray Diffraction Imaging: artefacts and sign convention in reconstructions. Scientific Reports, 2019, 9, 17357.	3.3	23
78	Water-Dispersible Copper Sulfide Nanocrystals via Ligand Exchange of 1-Dodecanethiol. Chemistry of Materials, 2019, 31, 541-552.	6.7	37
79	Interfacial charge transfer in Pt-loaded TiO2 P25 photocatalysts studied by in-situ diffuse reflectance FTIR spectroscopy of adsorbed CO. Journal of Photochemistry and Photobiology A: Chemistry, 2019, 370, 84-88.	3.9	19
80	CO oxidation by Pd supported on CeO2(100) and CeO2(111) facets. Applied Catalysis B: Environmental, 2019, 243, 36-46.	20.2	231
81	On the origin of the photocurrent of electrochemically passivated p-InP(100) photoelectrodes. Physical Chemistry Chemical Physics, 2018, 20, 14242-14250.	2.8	14
82	Low-temperature plasma-enhanced atomic layer deposition of 2-D MoS <sub>2</sub> : large area, thickness control and tuneable morphology. Nanoscale, 2018, 10, 8615-8627.	5.6	90
83	Stability of CoP <sub><i>x</i></sub> Electrocatalysts in Continuous and Interrupted Acidic Electrolysis of Water. ChemElectroChem, 2018, 5, 1230-1239.	3.4	35
84	Crystallographic orientation of facets and planar defects in functional nanostructures elucidated by nano-focused coherent diffractive X-ray imaging. Nanoscale, 2018, 10, 4833-4840.	5.6	14
85	Metalâ€Organic Frameworks as Catalyst Supports: Influence of Lattice Disorder on Metal Nanoparticle Formation. Chemistry - A European Journal, 2018, 24, 7498-7506.	3.3	29
86	Marrying SPR excitation and metal–support interactions: unravelling the contribution of active surface species in plasmonic catalysis. Nanoscale, 2018, 10, 8560-8568.	5.6	14
87	Interplay between Surface Chemistry, Precursor Reactivity, and Temperature Determines Outcome of ZnS Shelling Reactions on CuInS <sub>2</sub> Nanocrystals. Chemistry of Materials, 2018, 30, 2400-2413.	6.7	85
88	Tandem promotion of iron catalysts by sodium-sulfur and nitrogen-doped carbon layers on carbon nanotube supports for the Fischer-Tropsch to olefins synthesis. Applied Catalysis A: General, 2018, 568, 213-220.	4.3	17
89	Evaluating the Stability of Co <sub>2</sub> P Electrocatalysts in the Hydrogen Evolution Reaction for Both Acidic and Alkaline Electrolytes. ACS Energy Letters, 2018, 3, 1360-1365.	17.4	291
90	Pinpointing the active species of the Cu(DAT) catalyzed oxygen reduction reaction. Physical Chemistry Chemical Physics, 2018, 20, 19625-19634.	2.8	17

#	Article	IF	CITATIONS
91	Temperature-Dependent Kinetic Studies of the Chlorine Evolution Reaction over RuO <sub>2</sub> (110) Model Electrodes. ACS Catalysis, 2017, 7, 2403-2411.	11.2	111
92	Synthesis, Physicochemical Characterization, and Cytotoxicity Assessment of CeO <sub>2</sub> Nanoparticles with Different Morphologies. European Journal of Inorganic Chemistry, 2017, 2017, 3184-3190.	2.0	7
93	Probing the Influence of SSZâ€13 Zeolite Pore Hierarchy in Methanolâ€toâ€Olefins Catalysis by Using Nanometer Accuracy by Stochastic Chemical Reactions Fluorescence Microscopy and Positron Emission Profiling. ChemCatChem, 2017, 9, 3470-3477.	3.7	19
94	Role of Dissociatively Adsorbed Water on the Formation of Shallow Trapped Electrons in TiO <sub>2</sub> Photocatalysts. Journal of Physical Chemistry C, 2017, 121, 10153-10162.	3.1	24
95	Promoted Iron Nanocrystals Obtained via Ligand Exchange as Active and Selective Catalysts for Synthesis Gas Conversion. ACS Catalysis, 2017, 7, 5121-5128.	11.2	26
96	Role of Adsorbed Water on Charge Carrier Dynamics in Photoexcited TiO <sub>2</sub> . Journal of Physical Chemistry C, 2017, 121, 7514-7524.	3.1	82
97	Reactor for nano-focused x-ray diffraction and imaging under catalytic in situ conditions. Review of Scientific Instruments, 2017, 88, 093902.	1.3	7
98	Atomically Dispersed Pd–O Species on CeO <sub>2</sub> (111) as Highly Active Sites for Low-Temperature CO Oxidation. ACS Catalysis, 2017, 7, 6887-6891.	11.2	208
99	Effects of the Functionalization of the Ordered Mesoporous Carbon Support Surface on Iron Catalysts for the Fischer–Tropsch Synthesis of Lower Olefins. ChemCatChem, 2017, 9, 620-628.	3.7	50
100	Carbide-derived carbon aerogels with tunable pore structure as versatile electrode material in high power supercapacitors. Carbon, 2017, 113, 283-291.	10.3	171
101	Highâ€Efficiency InPâ€Based Photocathode for Hydrogen Production by Interface Energetics Design and Photon Management. Advanced Functional Materials, 2016, 26, 679-686.	14.9	69
102	Xâ€ray Excited Optical Fluorescence and Diffraction Imaging of Reactivity and Crystallinity in a Zeolite Crystal: Crystallography and Molecular Spectroscopy in One. Angewandte Chemie, 2016, 128, 7622-7626.	2.0	6
103	Bottlenecks limiting efficiency of photocatalytic water reduction by mixed Cd-Zn sulfides/Pt-TiO 2 composites. Applied Catalysis B: Environmental, 2016, 198, 16-24.	20.2	13
104	"Physical Chemistry of Solar Fuels Catalysis―— An Event for Early Career Researchers at the Max-Planck-Institute for Chemical Energy Conversion. ACS Energy Letters, 2016, 1, 353-355.	17.4	0
105	Synchrotron based operando surface Xâ€ray scattering study towards structure–activity relationships of model electrocatalysts. ChemistrySelect, 2016, 1, 1104-1108.	1.5	7
106	Enhanced Photoresponse of FeS <sub>2</sub> Films: The Role of Marcasite–Pyrite Phase Junctions. Advanced Materials, 2016, 28, 9602-9607.	21.0	64
107	ZrO <sub>2</sub> Is Preferred over TiO <sub>2</sub> as Support for the Ru-Catalyzed Hydrogenation of Levulinic Acid to γ-Valerolactone. ACS Catalysis, 2016, 6, 5462-5472.	11.2	169
108	Photoelectrochemistry: Enhanced Photoresponse of FeS2 Films: The Role of Marcasite-Pyrite Phase Junctions (Adv. Mater. 43/2016). Advanced Materials, 2016, 28, 9656-9656.	21.0	0

#	Article	IF	CITATIONS
109	Xâ€ray Excited Optical Fluorescence and Diffraction Imaging of Reactivity and Crystallinity in a Zeolite Crystal: Crystallography and Molecular Spectroscopy in One. Angewandte Chemie - International Edition, 2016, 55, 7496-7500.	13.8	14
110	Fluoride-assisted synthesis of bimodal microporous SSZ-13 zeolite. Chemical Communications, 2016, 52, 3227-3230.	4.1	36
111	Trimodal Porous Hierarchical SSZ-13 Zeolite with Improved Catalytic Performance in the Methanol-to-Olefins Reaction. ACS Catalysis, 2016, 6, 2163-2177.	11.2	116
112	Cu2O photoelectrodes for solar water splitting: Tuning photoelectrochemical performance by controlled faceting. Solar Energy Materials and Solar Cells, 2015, 141, 178-186.	6.2	72
113	Controlled Synthesis of Phaseâ€Pure Zeolitic Imidazolate Framework Coâ€ZIFâ€9. European Journal of Inorganic Chemistry, 2015, 2015, 1625-1630.	2.0	36
114	Quantitative 3D Fluorescence Imaging of Single Catalytic Turnovers Reveals Spatiotemporal Gradients in Reactivity of Zeolite H-ZSM-5 Crystals upon Steaming. Journal of the American Chemical Society, 2015, 137, 6559-6568.	13.7	69
115	Ex Situ and Operando Studies on the Role of Copper in Cu-Promoted SiO <sub>2</sub> –MgO Catalysts for the Lebedev Ethanol-to-Butadiene Process. ACS Catalysis, 2015, 5, 6005-6015.	11.2	95
116	On the Formation of Cd–Zn Sulfide Photocatalysts from Insoluble Hydroxide Precursors. Inorganic Chemistry, 2015, 54, 9491-9498.	4.0	14
117	Recent advances in secondary ion mass spectrometry of solid acid catalysts: large zeolite crystals under bombardment. Physical Chemistry Chemical Physics, 2014, 16, 5465-5474.	2.8	18
118	Synthesis of hierarchical zeolites using an inexpensive mono-quaternary ammonium surfactant as mesoporogen. Chemical Communications, 2014, 50, 14658-14661.	4.1	48
119	Large Zeolite Hâ€ZSMâ€5 Crystals as Models for the Methanolâ€toâ€Hydrocarbons Process: Bridging the Gap between Singleâ€Particle Examination and Bulk Catalyst Analysis. Chemistry - A European Journal, 2013, 19, 8533-8542.	3.3	29
120	In situ spectroscopic investigation of oxidative dehydrogenation and disproportionation of benzyl alcohol. Physical Chemistry Chemical Physics, 2013, 15, 12147.	2.8	43
121	Imaging the effect of a hydrothermal treatment on the pore accessibility and acidity of large ZSM-5 zeolite crystals by selective staining. Catalysis Science and Technology, 2013, 3, 1208-1214.	4.1	19
122	Electrospun Metal Oxide Nanofibres for the Assessment of Catalyst Morphological Stability under Harsh Reaction Conditions. ChemCatChem, 2013, 5, 2621-2626.	3.7	18
123	Intergrowth Structure and Aluminium Zoning of a Zeolite ZSMâ€5 Crystal as Resolved by Synchrotronâ€Based Micro Xâ€Ray Diffraction Imaging. Angewandte Chemie - International Edition, 2013, 52, 13382-13386.	13.8	51
124	Stability of Pt/γ-Al <sub>2</sub> O <sub>3</sub> Catalysts in Lignin and Lignin Model Compound Solutions under Liquid Phase Reforming Reaction Conditions. ACS Catalysis, 2013, 3, 464-473.	11.2	82
125	Synthesis and Morphology Control of AMâ€6 Nanofibers with Tailored â€Vâ€Oâ€V―Intermediates. Chemistry - A European Journal, 2013, 19, 14200-14204.	3.3	5
126	Adsorption of chlorine on Ru(0001)—A combined density functional theory and quantitative low energy electron diffraction study. Surface Science, 2012, 606, 297-304.	1.9	13

#	Article	IF	CITATIONS
127	One-dimensional confinement in heterogeneous catalysis: Trapped oxygen on RuO2(110) model catalysts. Surface Science, 2012, 606, L69-L73.	1.9	15
128	"Extracting―the Key Fragment in ETSâ€10 Crystallization and Its Application in AMâ€6 Assembly. Chemistry A European Journal, 2012, 18, 12078-12084.	- 3.3	8
129	Structure and Basicity of Microporous Titanosilicate ETS-10 and Vanadium-Containing ETS-10. Journal of Physical Chemistry C, 2012, 116, 17124-17133.	3.1	9
130	Near infrared emission spectrum of H13CN. Journal of Molecular Spectroscopy, 2010, 262, 75-81.	1.2	11
131	In situ studies of the oxidation of HCl over RuO2 model catalysts: Stability and reactivity. Journal of Catalysis, 2010, 272, 169-175.	6.2	54
132	Hydrogen-Promoted Chlorination of RuO <sub>2</sub> (110). Journal of Physical Chemistry C, 2010, 114, 10901-10909.	3.1	25
133	Dynamic response of chlorine atoms on a RuO2(110) model catalyst surface. Physical Chemistry Chemical Physics, 2010, 12, 15358.	2.8	28
134	Deacon Process over RuO2 and TiO2-Supported RuO2. , 2010, , 517-528.		0
135	Reaction Mechanism of the Oxidation of HCl over RuO <sub>2</sub> (110). Journal of Physical Chemistry C, 2008, 112, 9966-9969.	3.1	68
136	A spectrochemometric approach to tautomerism and hydrogen-bonding in 3-acyltetronic acids. Journal of Molecular Structure, 2006, 790, 80-88.	3.6	18
137	Von der Verbrennung zum Herzschlag: Chemische TriebkrÄfte. Chemie in Unserer Zeit, 2004, 38, 10-23.	0.1	0
138	Solar Driven Energy Conversion Applications Based on 3C-SiC. Materials Science Forum, 0, 858, 1028-1031.	0.3	13
139	Ru on Nâ€doped Carbon for the Selective Hydrogenolysis of Sugars and Sugar Alcohols. ChemCatChem, 0, , .	3.7	4